

High-sensitivity mass and position detection of micro-objects adhered to microcantilevers

Hui Xie · Julien Vitard · Sinan Haliyo ·
Stéphane Régnier

Received: 4 October 2007 / Revised: 2 January 2008 / Accepted: 19 February 2008
© Springer-Verlag 2008

Abstract A dynamic method for mass detection, considering attaching positions of micro-objects on microcantilevers, is introduced. Two models based on the Rayleigh–Ritz method were developed for analyses of the first flexural and the first torsional modes of a “cantilever–mass” system, respectively. Due to one-to-one correspondence between the longitudinal adhering positions of the micro-objects and the flexural resonant frequencies of the “cantilever–mass” system, the first model was employed for high-sensitivity mass detections of multi-object with different attaching positions on the cantilevers. The second model was developed for the analyses of links between the first torsional frequency of the “cantilever–mass” system and the transverse attaching positions of the micro-objects. Uniting these two models, the longitudinal and transverse attaching positions of one micro-object can be determined. Experimental results of polystyrene microspheres and ambrosia pollens attached on the microcantilever in the air validated the setup of the analytical models.

Keywords Mass detection · Microcantilever · Rayleigh–Ritz method · The first flexural mode · The first torsional mode

1 Introduction

Microcantilevers were introduced as nano-probes in the Atomic force microscope (AFM), which has been brought into the world for more than two decades [1], has been

proved to be a powerful tool in research and application of the nanotechnology. Not only can it be used for the characterization of micro and nano-samples, but also for nanofabrication through the AFM based manipulation. The origin application of AFM received many improvements, evolving from the measurement of the atomic roughness of a surface in both contact and non-contact modes, from the static (force) mode to the dynamic mode [2].

Among all research work relating to the microcantilevers, one particular kind of application is the high sensitivity mass detection by measuring resonant frequency shifts caused by an additional mass loaded on the cantilever. An early example for a cantilever–mass system was used to determine spring constants of AFM cantilevers by adding tungsten microspheres with known mass on the end of the cantilevers [3], and recently, a similar work presented an extension of the mass-added method by loading water microdrops generated by a commercial inkjet dispenser [4]. In contrast with static methods, the resonant frequency shift of the microcantilever provides higher sensitivity allowing mass detection in the attogram regime. Gradually, the resonant frequency shift of the cantilever beam, due to the mass adhered to the cantilever, has been widely used as a detection scheme for the small mass. A theoretical sensitivity on the attogram scale of a mass sensor was demonstrated by a simple linear electromechanical model for an electrostatically driven resonating cantilever [5]. Several micro or nano-cantilevers based on the silicon microfabrication technology, with sensitivities from femtogram to zeptogram have been developed [6–14]. The highly sensitive and convenient micro or nano-cantilevers were widely used in the biology area, including the detection of DNA, virus and cells [15–18]. Based on both detection of frequency shifts and bending of microcantilevers to measure mass changes as well as viscosity changes, novel

H. Xie (✉) · J. Vitard · S. Haliyo · S. Régnier
Institut des Systèmes Intelligents et Robotique (ISIR),
Université Pierre et Marie Curie–Paris 6/CNRS,
18 Route du Panorama-BP 61,
92265 Fontenay-Aux-Roses, France
e-mail: xie@robot.jussieu.fr

designs for gas and liquid sensing were presented [19, 20]. As an extremely sensitive method, the Anderson or vibration localization was employed in coupled microcantilevers to measure the added mass of a target analyte [21]. In [22], a dynamic method for mass detection was introduced, in which the attaching object is assumed as deformable and then its potential and kinetic energy were considered in the model based on Rayleigh–Ritz method. Even the hot nanomaterial carbon nanotube was also employed in this hot topic as a nanocantilever toward zeptogram detection [23].

In order to detect an accurate eigenfrequency of the cantilever–mass system, the additional moment of the added mass caused by defined position was taken into consideration through boundary conditions [8]. Considering the cell attaching position, a linearly approximate modification was introduced into the mass calculation [16]. In [18], a constant n was introduced in an algorithm for the mass calculation for the cases of the tip loading and uniform distribution on the cantilever, and a geometrical factor G was introduced into the same algorithm [7]. Aiming at high precision and special functions, cleverly designed structures, well defined parameters, special materials and new fabrication methods have been employed to improve the detecting sensitivity. However, note that most models and experiments assumed that micro and nano-objects were just placed on the very end of the microcantilever or some special defined attaching areas [8, 14]. A few researches paid attention to the adhering positions of the micro and nano-objects. In fact, unless the mass is accurately fabricated on a special position on the cantilever, other methods for the mass absorbing, accurately placing and distributing will undoubtedly bring positioning errors to the mass loading. Especially when the mass is directly distributed by micromanipulation, in which adhesion forces play a significant role in physical interactions between micro and nano-objects and the environment or the manipulator [24–26]. Although we can actively control and utilize the adhesion forces for micromanipulation [27, 28], the positioning errors will be induced in samples picking, releasing and locating tasks. Therefore, it is absolutely necessary to introduce a more accurate method for highly-sensitive mass detection.

In this paper, two dynamic models based on the Rayleigh–Ritz method were introduced, in which all dimensions of the microcantilever as well as the adhering positions of micro-objects were involved into the same model. The first model, considering the longitudinal position of micro-objects, was used for the highly precise mass detection and in the reverse way, for the longitudinal position measurement. The second one, taking into account the longitudinal and transverse positions of micro-objects

on the cantilever, was developed for the measurement of the transverse positions.

2 Theories and models

2.1 Model of the microcantilever

The Euler–Bernoulli theory is the most popular method for calculation of spring constants of microcantilevers based on experimental results. As shown in Fig. 1, the cantilever is built in at one end, free at the other end assumed to deform in the linear elastic range. L , w , and h are the length, width and the thickness of a rectangular cantilever, respectively. The coordinates are defined as follows: the origin is located on the centre of the cross section of the built-in end, the x -axis is along its length, and the z -axis and y -axis are along its thickness and the y -axis, respectively. The motion of flexural vibrations is a function of x :

$$EI_y(x) \frac{\partial^4 v}{\partial x^4} + \eta \rho S \frac{\partial v}{\partial t} + \rho S \frac{\partial^2 v}{\partial t^2} = 0 \tag{1}$$

where E is Young’s modulus of the silicon cantilever, $I_y = wh^3/12$ is its moment of inertia about the z -axis, $S = w \times h$ is its cross-section area, η is a damping constant and deflection function $v(z, t) = V(z)e^{i\omega t}$, ρ is the density of cantilever. Taking no account on the effect of the damping, the solutions of the equation is:

$$(K_n L)^3 [\cos(K_n L) \cos h(K_n L) + 1] = 0 \tag{2}$$

where K_n is the n th wave number of the cantilever ($K_1 L \approx 1.8751$ for the first flexural mode), The resonant frequencies are further obtained using the dispersion relation for n th flexural frequency in the cantilever:

$$\omega_n = (K_n L)^2 \sqrt{\frac{EI_y}{\rho S L^4}} \tag{3}$$

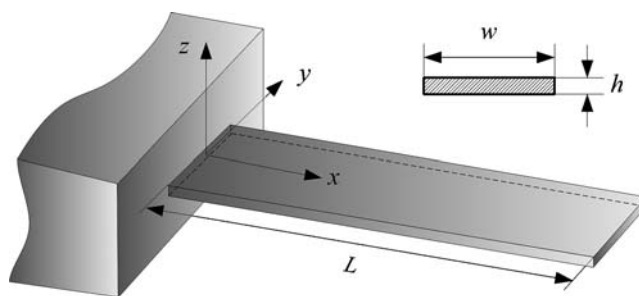


Fig. 1 The geometry model of the microcantilever

where ω_n is the n th flexural resonant frequency. If ω_n is known, so the thickness h of cantilever can be calculated by:

$$h = \frac{\omega_n}{K_n^2} \sqrt{\frac{12\rho}{E}}. \tag{4}$$

Thus the stiffness k of the cantilever can be also calculated by:

$$k = \frac{Ewh^3}{4L^3}. \tag{5}$$

The equation of the motion of the torsional modes is defined as [29]:

$$GJ \frac{\partial^2 \theta(x,t)}{\partial x^2} = \rho I_p \frac{\partial^2 \theta(x,t)}{\partial t^2} + c \frac{\partial \theta(x,t)}{\partial t} \tag{6}$$

where $\theta(x, t)$ is the rotation angle of the cantilever, G is the shear modulus, ρ is the density of the cantilever, c is the coefficient of viscous damping, $I_p = (wt^3 + w^3t)/12$ is the polar area moment of inertia and J is the torsional constant. For a rectangular cantilever, J can be obtained by [30]:

$$J \approx \frac{1}{3} wh^3 \left[1 - 0.63 \frac{h}{w} + 0.052 \left(\frac{h}{w} \right)^5 \right]. \tag{7}$$

The n th torsional frequency is obtained by:

$$\omega = \frac{(2n - 1)\pi}{2L} \sqrt{\frac{GJ}{\rho I_p}}, \quad n = 1, 2, \dots \tag{8}$$

2.2 Rayleigh–Ritz method

Hundreds of research articles and many books have appeared that used a method, termed ‘‘Rayleigh–Ritz method’’, to resolve natural frequencies of continuum systems, Although this was claimed that Rayleigh’s name should not be attached to the Ritz method, that is, the ‘‘Rayleigh–Ritz method’’ is an improper designation [31], the classic and perfect method will be employed to solve the natural frequencies of cantilever–mass system in our research. In Rayleigh’ method, potential (U) and kinetic (T) energies of the flexural system are considered to calculate the nature frequency of the system. The maximum U_{\max} and T_{\max} are defined:

$$U_{\max} = \frac{1}{2} \int_0^L EI(x) \left[\frac{\partial^2 z(x)}{\partial x^2} \right]^2 dx \tag{9}$$

$$T_{\max} = \frac{1}{2} \omega^2 \int_0^L \rho S(x) \left[\frac{\partial z(x)}{\partial t} \right]^2 dx \tag{10}$$

where E is the Young’s modulus of a continuum system, $I(x)$ is the moment of the inertia about the vibration, ρ is the density, $S(x)$ is the section area and $z(x)$ is the mode shape function. In this method, by assuming the mode shape, and setting the maximum values of potential and kinetic energy in a cycle of motion equal to each other, therefore, nature frequencies of the continuum system can be obtained by:

$$\omega^2 = \frac{\int_0^L EI(x) \left[\frac{\partial^2 z(x)}{\partial x^2} \right]^2 dx}{\int_0^L \rho S(x) \left[\frac{\partial z(x)}{\partial t} \right]^2 dx}. \tag{11}$$

It is very clear that the calculation accuracy strongly depends on how closely the assumed mode shape fits the exact one. In Ritz’s method, a displacement function is assumed in terms of a series of admissible displacement functions having undetermined coefficients, and then minimizes an energy functional involving U and T to determine frequencies. The mode function is defined by:

$$v(x) = \sum_{i=0}^n a_i \varphi_i(x) \tag{12}$$

where the $\varphi_i(x)$ is algebraic polynomials or trigonometric functions and the a_i are arbitrary coefficients, which is determined by partial derivatives of Eq. 11, for the calculation if the minimum frequency:

$$\frac{\partial \omega^2}{\partial a_i} = 0 \quad (i = 1, 2, \dots, n). \tag{13}$$

From the Eqs. 11 and 12, a similar equation for the nature frequency is obtained:

$$\omega^2 = \frac{\{a\}^T [K] \{a\}}{\{a\}^T [M] \{a\}} = \frac{\mathbf{K}}{\mathbf{M}} \tag{14}$$

where $\{a\}^T = \{a_1, a_2, \dots, a_n\}$, \mathbf{K} and \mathbf{M} are stiffness and mass matrixes, respectively. According to the Eq. 13, the solution of the nature frequency is given by:

$$[\mathbf{K} - \omega^2 \mathbf{M}] \{a\} = 0. \tag{15}$$

Thus for the arbitrary coefficients $\{a\}$, the solution is:

$$\det(\mathbf{K} - \omega^2 \mathbf{M}) = 0. \tag{16}$$

For a complex system consisting of multi-subsystems, for example the spring bearing and mass adhering to the vibrating continuum systems, the additional potential (U) and kinetic (T) energies should be added to the whole system. Therefore, in the ‘‘cantilever–mass’’ system, adding the kinetic (T) energy of micro and nano-objects to the whole system, the nature frequency of the whole system can be accurately obtained.

2.3 Analysis for flexural vibration

A classic formulation was widely used to calculate the micro mass by measuring the frequency shifts [32]:

$$\Delta m = \frac{k}{4n\pi^2} \left(\frac{1}{f_{\text{mass}}^2} - \frac{1}{f_{\text{res}}^2} \right) \quad (17)$$

where k is the stiffness of the cantilever, Δm is the small mass should be measured, f_{res} and f_{mass} are the resonant frequency of the cantilever with and without mass loading, respectively. The variable $n=1$ in the case the added mass is placed right on the tip and $n=0.24$ when the additional mass is uniformly distributed on the microcantilever [32]. However, for the mass detection of one object or several objects haphazardly attaching to the cantilever, a more complex model should be developed.

Another method, considering the attaching position, a linearly approximate modification was introduced into the mass calculation of a single cell [16]:

$$\Delta f = 0.279m_{\text{add}} \frac{x}{l} \sqrt{\frac{EI}{l^3 m_0^3}} \quad (18)$$

where l and I are the length and the moment of inertia of the microcantilever, respectively; m_{add} is mass of a attaching cell, x is the position of the cell measured from the base of the cantilever, and m_0 is the mass of the microcantilever.

The ‘‘cantilever–mass’’ system is obviously distinct from the cantilever alone. In our research, Rayleigh–Ritz method is employed to solve this complex problem. Considering that there is no energy loss between the object and the cantilever, the ‘‘cantilever–mass’’ system is modeled as in Fig. 2. In this model, as an example, three microspheres, adhering to the position l_{kx} , have the mass of m_k . In the case of the first resonant mode of deflection, the shape function $z_f(x)$ can be given by:

$$z_f(x) = f_1\varphi_1(x) + f_2\varphi_2(x) \quad (19)$$

where $\varphi_1(x)$ and $\varphi_2(x)$ is defined as x^2 and x^3 , respectively, f_1 and f_2 are two corresponding constants. So the maximum

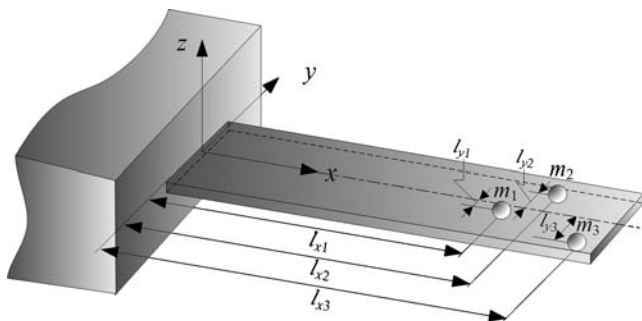


Fig. 2 The geometry model of the ‘‘cantilever–mass’’ system. An example of three microspheres m_1 , m_2 and m_3 adhering on the cantilever have coordinates of (l_{x1}, l_{y1}) , (l_{x2}, l_{y2}) and (l_{x3}, l_{y3}) , respectively

potential (U_f) and maximum kinetic (T_f) energies of the cantilever under the flexural modes are given by:

$$U_f = \frac{1}{2}EI_y \int_0^L \left[\sum_{i=1}^2 f_i \frac{\partial \varphi_i^2(x)}{\partial x^2} \right] \left[\sum_{j=1}^2 f_j \frac{\partial \varphi_j^2(x)}{\partial x^2} \right] dx \quad (20)$$

$$T_f = \frac{1}{2}\rho S\omega^2 \int_0^L \left[\sum_{i=1}^2 f_i \varphi_i(x) \right] \left[\sum_{j=1}^2 f_j \varphi_j(x) \right] dx \quad (21)$$

where ρ is the density of cantilever, S is the section of area. So the elements of the matrix \mathbf{K} and \mathbf{M} are:

$$k_{ij} = EI_y \int_0^L \frac{\partial^2 \varphi_i(x)}{\partial x^2} \times \frac{\partial^2 \varphi_j(x)}{\partial x^2} dx \quad (22)$$

$$m_{ij} = \rho S \int_0^L \varphi_i(x) \times \varphi_j(x) dx. \quad (23)$$

For the attaching objects, the elements are given by:

$$m_{ij \text{ object}} = \sum_{k=1}^N m_k \varphi_i(l_{kx}) \times \varphi_j(l_{kx}) \quad (24)$$

where k is the serial number of the N micro-objects. So the mass matrix \mathbf{M} and the stiffness \mathbf{K} for the flexural mode of the whole system are obtained:

$$\mathbf{M} = \begin{bmatrix} \frac{1}{5}\rho SL^5 + \sum_{k=1}^N m_k l_{kx}^4 & \frac{1}{6}\rho SL^6 + \sum_{k=1}^N m_k l_{kx}^5 \\ \frac{1}{6}\rho SL^6 + \sum_{k=1}^N m_k l_{kx}^5 & \frac{1}{7}\rho SL^7 + \sum_{k=1}^N m_k l_{kx}^6 \end{bmatrix} \quad (25)$$

$$\mathbf{K} = \begin{bmatrix} 4EIL & 6EIL^2 \\ 6EIL^2 & 12EIL^3 \end{bmatrix}. \quad (26)$$

From Eq. 16, a solution in the case of multi-object attached to the cantilever, including attaching position l_{kx} , resonant frequency ω and m_k , is obtained:

$$f(l_{kx}, m_k, \omega) = 0 \quad (k = 1, 2, \dots, N). \quad (27)$$

Note that there are three variables in Eq. 27, so at least two of them are needed to resolve the equation. For example, if we know the attaching position l_{kx} of the multi-object and the resonant frequency ω of the ‘‘cantilever–mass’’ system, the mass m_k of the objects can be calculated, and also if the mass of the object and the resonant frequency are known (just for one object), so the attaching position of the object on the x axis can be easily obtained.

2.4 Analysis for the first torsional vibration

For torsional models, the “cantilever–mass” system is also modeled as in Fig. 2. The torsional axis is along the x axis and through the centre of the cross section of the built-in end. In the first torsional model, the shape function $z_t(x)$ is given by:

$$z_t(x) = t_1\psi_1(x) + t_2\psi_2(x) \tag{28}$$

where $\psi_1(x)$ and $\psi_2(x)$, the functions of the torsional angle, are x and x^2 , respectively, t_1 and t_2 are two corresponding constants. So the maximum potential (U_t) and maximum kinetic (T_t) energies of the beam are:

$$U_t = \frac{1}{2} GJ \int_0^L \left[\sum_{i=1}^2 t_i \frac{\partial \psi_i(x)}{\partial x} \right] \left[\sum_{j=1}^2 t_j \frac{\partial \psi_j(x)}{\partial x} \right] dx \tag{29}$$

$$T_t = \frac{1}{2} \rho I_p \omega^2 \int_0^L \left[\sum_{i=1}^2 t_i \psi_i(x) \right] \left[\sum_{j=1}^2 t_j \psi_j(x) \right] dx \tag{30}$$

where ρ is the density of cantilever, $I_p = (wt^3 + w^3t)/12$ is the polar area moment of inertia, J is the torsional constant, which can be obtained by Eq. 7. So the factors of the matrix \mathbf{K} and \mathbf{M} for the torsional mode are:

$$k_{ij} = GJ \int_0^L \frac{\partial \psi_i(x)}{\partial x} \times \frac{\partial \psi_j(x)}{\partial x} dx \tag{31}$$

$$m_{ij} = \rho I_p \int_0^L \psi_i(x) \times \psi_j(x) dx. \tag{32}$$

To the attaching objects, the elements are given by:

$$m_{ijobject} = \sum_{k=1}^N J_{mk} \psi_i(x) \times \psi_j(x) \tag{33}$$

where k is the serial number of the N micro and nano-objects J_m is the inertia moment of mass. To the microsphere:

$$J_m = \frac{2}{5} mr^2 + m \left[l_{ky}^2 + \left(\frac{t}{2} + r \right)^2 \right] \tag{34}$$

where r is the radius of the attaching object. So the mass matrix \mathbf{K} of the first torsional model are obtained by:

$$\mathbf{M} = \left[\begin{array}{c} \frac{1}{3} \rho I_p L^3 + \sum_{k=1}^N J_{mk} l_{kx}^2 \quad \frac{1}{4} \rho I_p L^4 + \sum_{k=1}^N J_{mk} l_{kx}^3 \\ \frac{1}{4} \rho I_p L^4 + \sum_{k=1}^N J_{mk} l_{kx}^3 \quad \frac{1}{5} \rho I_p L^5 + \sum_{k=1}^N J_{mk} l_{kx}^4 \end{array} \right] \tag{35}$$

$$\mathbf{K} = \left[\begin{array}{cc} GJL & GJL^2 \\ GJL^2 & \frac{4}{3} GJL^3 \end{array} \right]. \tag{36}$$

A solution in case of one object attached to the cantilever, including inertia moment l_{kx} , J_{mk} and resonant frequency ω , is obtained by:

$$f(l_{kx}, J_{mk}, \omega) = 0 \quad (k = 1, 2, \dots, N). \tag{37}$$

There are three variables in Eq. 37 at least two of them is needed to resolve the equation. For example, if we know the l_x and inertia moment of mass J_m , which is determined by the mass m_k and its position l_{ky} , to the torsional axis, then the resonant frequency of the “cantilever–mass” system can be calculated. And also if the mass of the object, the first flexural and torsional resonant frequencies of the “cantilever–mass” system are known (just for one object), so the attaching position of the object can be easily obtained, wherein first flexural and torsional resonant frequency are used for the measurement of the position on x and y axis respectively.

3 Experiments and results

3.1 Set-up of micromanipulator

The experimental micromanipulator consists of a support, a microcantilever, a piezoceramic and a laser beam deflection system. Generally, due to the fabrication errors, the spring constant of the cantilever varies from others fabricated on the different chips. As the cube of the thickness and length, and as a result dimensional errors induce large errors on the spring constant. Thus, accurate force calibration should be required for the characterization of each cantilever.

The PI-89 piezoceramic has a thickness of 1 and 5 and 8 mm in width and length, respectively. A signal generator has been used to actuate the piezoceramic, which can produce sine waves ranging from 0 to 20 V, with bandwidth ranging from 1 to 3 MHz and accuracies of 1 Hz from 0 to 10 kHz, 10 Hz below 1 MHz, 100 Hz within the range of 1 M–3 MHz. The flexural and torsional vibrations of microcantilever are detected by a laser deflection beam and a four-quadrant photo detector with a lock-in amplifier.

3.2 Calibration of the microcantilever

The scientific community needs a rapid and reliable way of accurately determining the stiffness of AFM cantilevers. Many methods, including the dynamic method (forced and thermal oscillation), static loading and FEA methods were widely used to calibrate the stiffness of the cantilever [33]. In [34], a hybrid method is introduced for the calibration of the spring constants of atomic force microscopy cantilevers.

To the proposed method, the key parameters of the cantilever are the thickness and the first torsional resonant frequency of the cantilever. If the first resonant frequency of the cantilever is determined, the thickness of the cantilever can be easily obtained.

The experiment cantilevers have wedge-shaped tip as in Fig. 3a, in order to take into account the effect of wedge-shaped tip of the cantilever, the Eqs. 22 and 23 should be modified for the flexural model:

$$k_{ij} = EI_y \int_0^{L-l_w} \frac{\partial^2 \varphi_i(x)}{\partial x^2} \times \frac{\partial^2 \varphi_j(x)}{\partial x^2} dx + EI_y \int_{L-l_w}^L \frac{(L-x)}{l_w} \times \frac{\partial^2 \varphi_i(x)}{\partial x^2} \times \frac{\partial^2 \varphi_j(x)}{\partial x^2} dx \quad (38)$$

$$m_{ij} = \rho S \int_0^{L-l_w} \varphi_i(x) \times \varphi_j(x) dx + \rho S \times \int_{L-l_w}^L \frac{(L-x)}{l_w} \times \varphi_i(x) \cdot \varphi_j(x) dx \quad (39)$$

where l_w is the height of the wedge tip on the x axis. So if the first flexural frequency of the cantilever is known, the thickness of the cantilever can be calculated by the modified Eq. 27 (set $m=0$). The length and width of the cantilever were measured as 598 and 141 μm for the stiffness calculation. The experimental results show that fabrication errors of microcantilevers resulting in great differences between the measured parameters and commercially provided ones. This indicates the necessarily of the calibration of cantilevers to the accurate applications. In the following experiments, the cantilever with stiffness of 20.15 N/m was selected.

3.3 Detection of mass and longitudinal positions

In the experiments, the natural frequency of the “cantilever–mass” system was measured using a low magnitude variable frequency sinusoidal excitation and observing the output signal of the microcantilever by the laser beam deflection system. This output signal is the maximum when the frequency of excitation equals to the natural frequency of the system. In order to validate the relationships among the resonant frequencies, attaching position of the microsphere on the x axis (longitude position) and mass of the microsphere, as shown in Fig. 3a, another AFM tip was used to roll a polystyrene microsphere (with a diameter of 22.5 μm) to locate it on eight positions from the tip of the cantilever to the near area of the stain gauge of the cantilever [35], as shown in Fig. 3b.

As shown in Fig. 4a, the measured mass of the polystyrene microsphere is $(6.3553 \pm 0.2498) \times 10^{-12}$ kg which was calculated from the average value of the first seven results (red circles), in which the longitudinal positions of microsphere were measured by microscopic vision under a magnification of $\times 20$ with a resolution of 0.55 $\mu\text{m}/\text{pixel}$. The result is consistent with the theoretical mass values (with a density of 1,040–1,060 kg/m^3). But for the method represented in Eq. 18, the results are not satisfactory (black diamonds) due to the algorithm itself, in which a simple linear compensation for the position errors of the attaching objects was used. Note that in our experiments, when the position was on 147 μm , near the built-in end of the cantilever, a negative value was

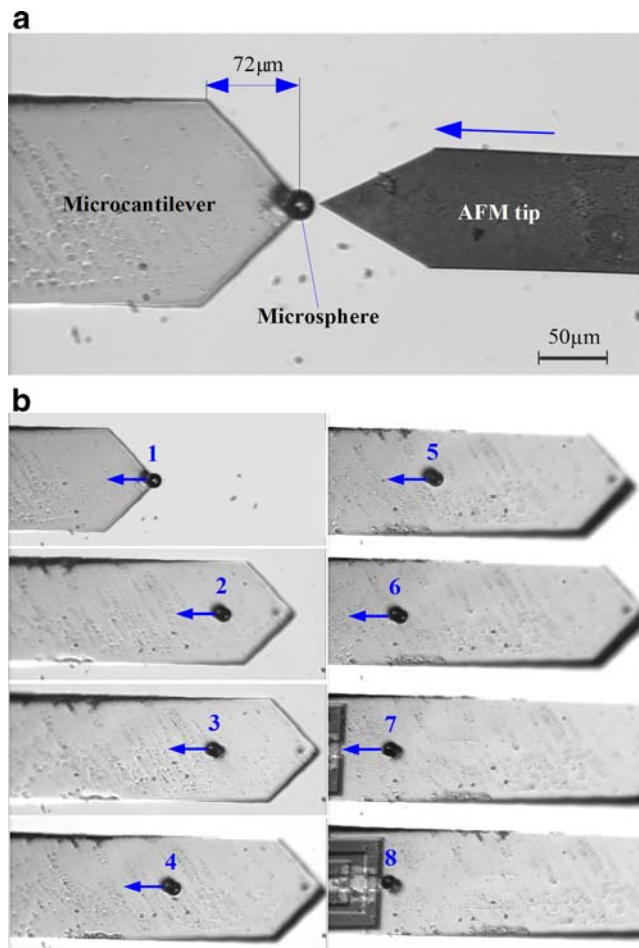


Fig. 3 Placing of the microsphere. **a** Illustration of the placing, in which another AFM cantilever was used to locate the microsphere to certain positions. **b** The microsphere on eight different positions along the x axis

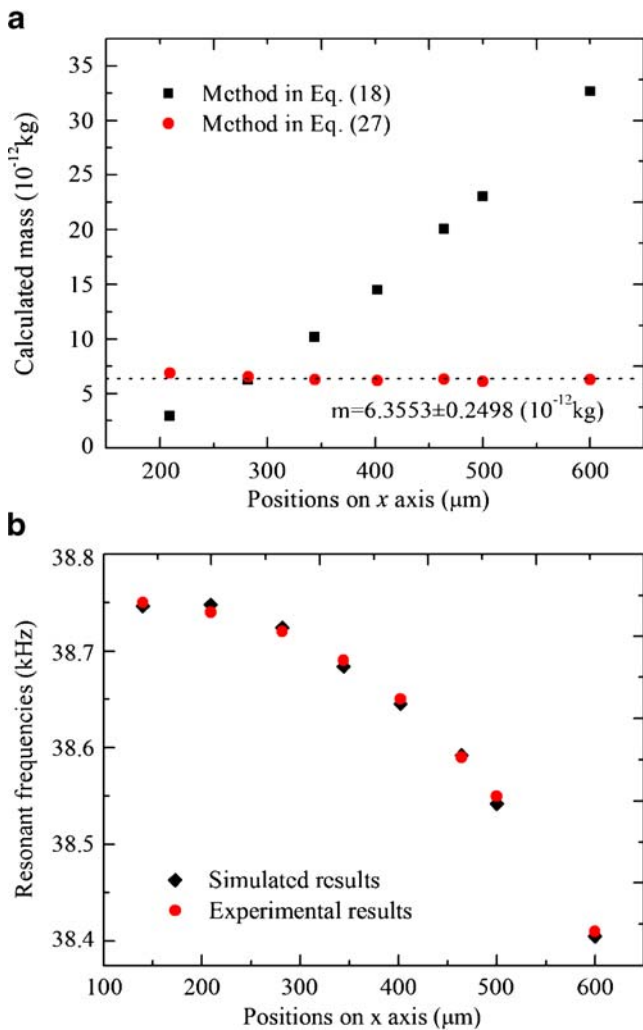


Fig. 4 a Experimental results using Eq. 18 (black diamonds) and Eq. 27 (red circles). b A position–frequency curve of the “cantilever–microsphere” system. These values were obtained by simulations (black diamonds) and experiments (red circles)

obtained due to low sensitivity of the mass detection near the root of the cantilever and the low resolution of the signal generator (10 Hz), that is when the polystyrene microsphere is placed in this location, the frequency shift of the microcantilever is less than 10 Hz. This problem can be resolved by using the signal generator with a higher resolution or other microcantilevers with higher sensitivities of mass detection.

The experiments showed that the resonant frequencies of the system strongly depended on the attaching positions of the microsphere. Figure 4b shows that the resonant frequency of the “cantilever–microsphere” system nonlinearly reduces when the position of the microsphere increases along the x axis (red circles), which is consistent with the simulated results (black diamonds, using measured mass 6.2475×10^{-12} kg).

Using the method in Eq. 17 as the mass placed on the tip, a measured mass 6.2045×10^{-12} was obtained using the stiffness 20.15 N/m calculated by the proposed calibration method, and 9.0277×10^{-12} generated from the stiffness 29.32 N/m. The former result is almost near the real mass of the microsphere, but the later one has a measured error of about 46%. These results reaffirm the significant contribution of the wedge-shaped tip to the nature frequencies of the cantilever. If we set the $m=0$ and frequency 38.75 kHz in Eq. 27, the stiffness of the cantilever is also accurately measured as 20.15 N/m.

Figure 5 shows that four same polystyrene microspheres were placed on the back surface of the cantilever with different positions on x axis. Their positions $l_1=522 \mu\text{m}$, $l_2=490 \mu\text{m}$, $l_3=509 \mu\text{m}$ and $l_4=533 \mu\text{m}$ were measured by microscopic vision with a resolution of $0.55 \mu\text{m}/\text{pixel}$. The mass 6.3159×10^{-12} kg was calculated by Eq. 27. In contrast, using the conventional method described in Eq. 17 and the same resonant frequency 37.88 kHz, the mass is 5.4036×10^{-12} kg, leading an measurement difference of 14.4% due to the attaching position errors of microspheres, which are not on the very end of the cantilever.

3.4 Detection of transverse positions

In the torsional vibration experiments, in order to validate the relationships among the resonant frequencies, attaching positions and mass of the microobjects, as shown in Fig. 6, a single ambrosia pollen (with a diameter of 20–21 μm) was released on 14 different positions along the y axis of cantilever. The natural frequency of the “cantilever–mass” system was measured using a sinusoidal excitation with a very low magnitude, because the micro-object easily escapes from the end-effector with a high frequency (the first torsional resonant frequency of the cantilever is 284.7 kHz) [22]. Experimental results showed that torsional resonant frequencies strongly depend on the attaching positions of micro-objects. As shown in the Eq. 37, the resonant frequency

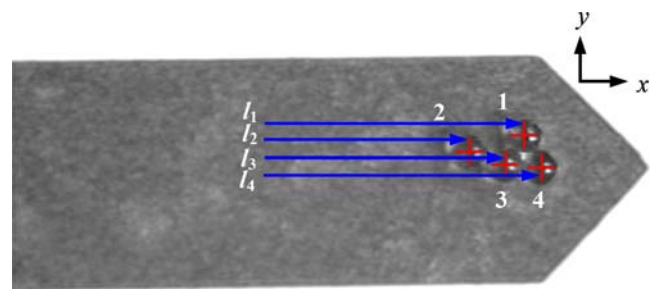


Fig. 5 Four microspheres adhere to the cantilever with positions of l_1 , l_2 , l_3 and l_4 on x axis, respectively. The positions are measured by the microscopic vision with a resolution of $0.55 \mu\text{m}/\text{pixel}$

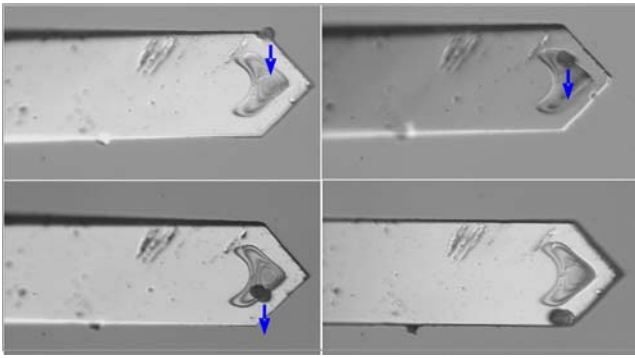


Fig. 6 The ambrosia pollen was released on different positions along the y axis on the microcantilever

of “cantilever–mass” system was determined by the position on x , y axis and mass of the ambrosia pollen. This problem was resolved as follows: firstly, the ambrosia pollen was placed on the tip of the cantilever and then the mass was measured as 3.8476×10^{-12} kg. Secondly, the first flexural and torsional resonant frequency of the “cantilever–mass” system was detected, and then the method in Eq. 27 was used to calculate the coordinate of the ambrosia pollen on the x axis. Subsequently, all the variables were obtained excepting for the transverse position of the ambrosia pollen on the y axis, which could be easily obtained by proposed method described in the Eq. 37. Because the torsion is symmetrical to the torsional axis, two calculation results (positive and negative) with the same absolute value should be obtained, so some other methods, such as vision, should be used to determine the real positions of the pollen. The corresponding experimental results are shown in Table 1. In order to validate the proposed method, the microscopic vision was also employed to measure the positions. The comparison shows that

Table 1 Experimental results of position measurement of the ambrosia pollen adhered to the cantilever

Positions	Dynamic method; x, y (μm)	Microscopy vision; x, y (μm)	Error; Δx , Δy (μm)
1	512.2, 67.7	510.8, 66.8	1.4, 0.9
2	507.2, 58.6	508.0, 57.2	-0.8, 1.4
3	510.1, 49.8	511.9, 51.7	-1.8, -1.9
4	513.5, 40.5	512.4, 38.2	1.1, 2.3
5	515.4, 24.8	514.6, 26.1	0.8, -1.3
6	524.8, 6.0	523.4, 9.2	1.4, -3.2
7	510.4, 4.1	511.3, 0.8	-0.9, 3.3
8	496.6, -3.5	495.4, -6.9	1.2, 3.4
9	525.2, -12.1	526.1, -14.7	-0.9, 2.6
10	483.5, -27.9	484.3, -26.8	-0.8, -1.1
11	507.8, -32.4	508.4, -31.6	-0.6, -0.8
12	497.5, -44.2	496.5, -42.2	1.0, -2.0
13	516.1, -54.9	514.5, -55.8	1.6, 0.9
14	521.8, -64.0	523.4, -65.4	-1.6, 1.4

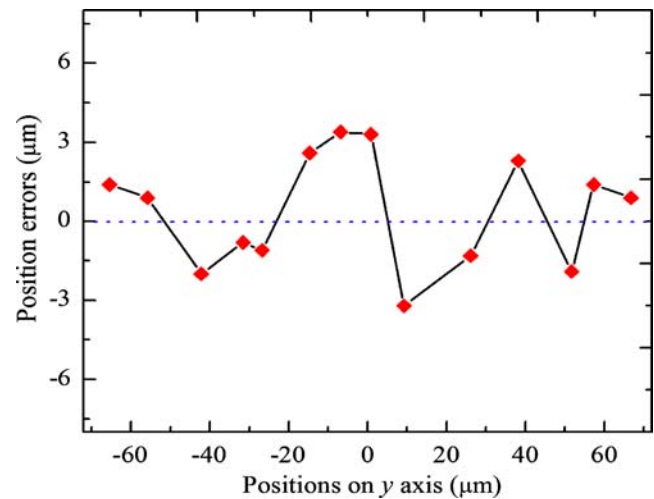


Fig. 7 Measured errors of y positions generated by the method in Eq. 37 compared with results determined by microscopy vision

differences between these two groups of results are acceptable. Note that the measurement results are more imprecise when the adhering position is approaching the torsional axis, as shown in Fig. 7, where the mass detection sensitivity is less than that of the attaching locations away from the torsional axis.

4 Conclusions

Two models based on the Rayleigh–Ritz theory for the mass detection and position calculation of the micro and nano-objects adhered to the microcantilevers were introduced. For the mass measurement, one model for the flexure mode of the “cantilever–mass” system was developed. Unlike the conventional method, not only can this method be used for the mass measurement of multi-objects with help of microscopy vision, also the positions of the object on the longitudinal axis of the cantilever can be accurately detected. Another model for the torsional mode of the “cantilever–mass” system was proposed for the detection of the position on transverse axis. In the actual use, once the longitudinal positions of micro-objects and the resonant frequency of cantilever are known, the mass of can be precisely determined by the first mode. In a contrary manner, If the mass and the first flexure and the first torsion resonant frequency are know, based on these two models, the adhering position of the micro-object follows can be easily obtained. These two models can be employed together for the mass measurement and position detection of the objects adhered to the microcantilevers.

Acknowledgment This work has been partially supported by the European project NANORAC (No. STRP 013680).

References

- Binning G, Quate CF, Gerber C (1986) Atomic force microscope. *Phys Rev Lett* 56:930–933
- Bhushan B (2004) Springer handbook of nanotechnology. Springer, Berlin
- Cleveland JP, Manne S (1993) A nondestructive method for determining the spring constant of cantilevers for scanning force microscopy. *Rev Sci Instrum* 64:403–405
- Golovko DS, Haschke T, Wiechert W, Bonaccorso E (2007) Nondestructive and noncontact method for determining the spring constant of rectangular cantilevers. *Rev Sci Instrum* 78:43705
- Abadal G, Davis ZJ, Helbo B, Borrise X, Ruiz R, Boisen A, Campabadal F, Esteve J, Figueras E, Perez-Murano F, Barniol N (2001) Electromechanical model of a resonating nano-cantilever-based sensor for high-resolution and high-sensitivity mass detection. *Nanotechnology* 12:100–104
- Davis ZJ, Abadal G, Kuhn O, Hansen O, Grey F, Boisen A (2000) Fabrication and characterization of nanoresonating devices for mass detection. *J Vac Sci Technol* 18:612–616
- Lavrik VN, Datskos PG (2003) Femtogram mass detection using photothermally actuated nanomechanical resonators. *Appl Phys Lett* 82:2697–2699
- Teva J, Abadal G, Torres F, Verd J, Pérez-Murano F, Barniol N (2005) A femtogram resolution mass sensor platform, based on SOI electrostatically driven resonant cantilever. Part I: electromechanical model and parameter extraction. *Ultramicroscopy* 106:800–807
- Ilica B, Craighead HG, Krylov S, Senaratne W, Ober C, Neuzil P (2004) Attogram detection using nanoelectromechanical oscillators. *J Appl Phys* 95:3694–703
- Jin DZ, Li XX, Liu J, Zuo GM, Wang YL, Liu M, Yu HT (2006) High-mode resonant piezoresistive cantilever sensors for tens-femtogram resolvable mass sensing in air. *J Micromechanics Microengineering* 16:1017–1023
- Arlett JL, Maloney JR, Gudlewski B, Muluneh M, Roukes ML (2006) Self-sensing micro- and nanocantilevers with attonewton-scale force resolution. *Nano Lett* 6:1000–1006
- Hosaka S, Chiyoma T, Ikeuchi A, Okano H, Sone H, Izumi T (2006) Possibility of a femtogram mass biosensor using a self-sensing cantilever. *Current Applied Physics* 6:384–388
- Shen ZY, Shih WY, Shih WH (2006) Self-exciting, self-sensing $\text{PbZr}_{0.53}\text{Ti}_{0.47}\text{O}_3/\text{SiO}_2$ piezoelectric microcantilevers with femtogram/Hertz sensitivity. *Appl Phys Lett* 89:023506
- Yang YT, Callegari C, Feng XL, Ekinci KL, Roukes ML (2006) Zeptogram-scale nanomechanical mass sensing. *Nano Lett* 6:583–586
- Su M, Li SY, Dravid VP (2003) Microcantilever resonance-based DNA detection with nanoparticle probes. *Appl Phys Lett* 82:3562–3564
- Ilic B, Czaplewski D, Zalalutdinov M, Craighead HG (2001) Single cell detection with micromechanical oscillators. *J Vac Sci Technol B* 19:2825–2828
- Gupta A, Akin D, Bashir R (2003) Single virus particle mass detection using microresonators with nanoscale thickness. *Appl Phys Lett* 84:1976–1978
- Gupta A, Akin D (2004) Detection of bacterial cells and antibodies using surface micromachined thin silicon cantilever resonators. *J Vac Sci Technol B* 22:2785–2791
- Vidic A, Then D, Ziegler CH (2003) A new cantilever system for gas and liquid sensing. *Ultramicroscopy* 97:407–416
- Hagleitner C, Hierlemann A, Lange D, Kummer A, Kerness N, Brand O, Baltes H (2001) Smart single-chip gas sensor microsystem. *Nature* 414:293–296
- Spletzer M, Raman A, Wu AQ, Xu XF (2006) Ultrasensitive mass sensing using mode localization in coupled microcantilevers. *Appl Phys Lett* 88:254102
- Haliyo S, Régnier S, Guinot JC (2003) [mü] MAD, the adhesion based dynamic micromanipulator. *Eur J Mech A, Solids* 22:903–916
- Nishio M, Sawaya S, Akita S, Nakayama Y (2005) Carbon nanotube oscillators toward zeptogram detection. *Appl Phys Lett* 86:133111
- Rollot Y, Régnier S, Guinot JC (1999) Simulation of micro-manipulations: adhesion forces and specific dynamic models. *Int J Adhes Adhes* 19:35–48
- Rollot Y, Régnier S, Guinot JC (2002) Dynamical model for the micro-manipulation by adhesion: experimental validations for determined conditions. *J Micromechatronics* 1:273–297
- Lambert P, Régnier S (2006) Surface and contact forces models within the framework of microassembly. *J Micromechatronics* 3:123–157
- Zhou Q, Aurelian A, Chang B, Corral C, Koivo NK (2002) Microassembly system with controlled environment. *J Micromechatronics* 2:227–248
- Driesen W, Varidel T, Régnier S, Breguet JM (2005) Micro manipulation by adhesion with two collaborating mobile micro robots. *J Micromechanics Microengineering* 15:S259–S267
- Gorman DJ (1975) Free vibration analysis of beams and shafts. Wiley, New York
- Ross CTF (1991) Finite element programs for structural vibrations. Springer, London
- Leissa AW (2005) The historical bases of the Rayleigh and Ritz methods. *J Sound Vib* 287:961–978
- Chen GY, Thundat T, Wachter EA, Warmack RJ (1995) Adsorption-induced surface stress and its effects on resonance frequency of microcantilevers. *J Appl Phys* 77:3618–3622
- Burnham NA, Chen X, Hodges CS, Matei GA, Thoreson EJ, Roberts CJ, Davies MC, Tandler SJB (2003) Comparison of calibration methods for atomic-force microscopy cantilevers. *Nanotechnology* 14:1–6
- Mendels DA, Lowe M, Cuenat A, Cain MG, Vallejo E, Ellis D, Mendels F (2006) Dynamic properties of AFM cantilevers and the calibration of their spring constants. *J Micromechanics Microengineering* 16:1720–1723
- Haliyo DS, Dionnet F, Régnier S (2006) Controlled rolling of microobjects for autonomous manipulation. *J Micromechatronics* 3:75–101